Cell Motility Resulting from Spontaneous Polymerization Waves

K. Doubrovinski
Theoretische Physik, Universität des Saarlandes, 66041 Saarbrücken, Germany
and Department of Molecular Biology, Princeton University, Princeton, New Jersey 08544, USA

K. Kruse
Theoretische Physik, Universität des Saarlandes, 66041 Saarbrücken, Germany
(Received 3 January 2011; published 16 December 2011)

The crawling of cells on a substrate is in many cases driven by the actin cytoskeleton. How actin filaments and associated proteins are organized to generate directed motion is still poorly understood. Recent experimental observations suggest that spontaneous cytoskeletal waves might orchestrate the actin-filament network to produce directed motion. We investigate this possibility by studying a mean-field description of treadmilling filaments interacting with nucleating proteins, a system that is known to self-organize into waves. Confining the system by a boundary that shares essential features of membranes, we find that spontaneous waves can generate directional motion. We also find that it can produce lateral waves along the confining membrane as are observed in spreading cells.

DOI: 10.1103/PhysRevLett.107.258103 PACS numbers: 87.17.Jj, 87.16.Ln

The migration of cells on substrates plays an important role during development, immune responses, and wound healing [1]. During the past two decades a large number of molecules essential for cell crawling have been identified and some of them have been characterized biochemically in impressive detail [2]. This inventory of proteins notably implies actin, which can assemble into filamentous polymers. The two ends of an actin filament display different assembly kinetics, which can lead to "treadmilling," where the filament grows at one and shrinks at the other end. However, in spite of our molecular understanding, the way in which interactions between actin and other cytoskeletal proteins lead to their organization on a cellular scale and generate directed motion remains largely unknown.

Several physical approaches operating on different scales have been developed in the past to elucidate different aspects of cell crawling. A large body of work has followed rather microscopic approaches to study the generation of forces by polymerization of actin filaments [3]. Large scale phenomenological approaches have been used to set up whole cell models [4,5] or to describe general aspects of the force generating cell structures [6–10]. Most of these approaches did not offer an explanation of how a cell acquires directionality, because it was built in by assuming predefined leading and trailing edges, which might be appropriate in the presence of external cues.

Remarkably, however, directed motion does not necessarily require an external guiding stimulus. Instead, cells can polarize spontaneously [11]. Usually this is attributed to feedback loops in signaling pathways, which have been analyzed from a computational point of view in a number of works [12–15]. A mechanism for spontaneous cell polarization resulting from a mechanical instability of the cytoskeleton has been presented by Callan-Jones *et al.* using a coarse-grained phenomenological description [16]. An alternative possibility has been suggested by observations on naive human neutrophil granulocytes, which are a kind of white blood cells. There, spontaneous actin polymerization waves have been observed and were argued to orchestrate cytoskeletal proteins to generate directional cell motility [17]. Spontaneous actin waves are now recognized to be a common cellular phenomenon [18] and a number of possible underlying mechanisms have been studied [17,19–22]. While these works study mechanisms of wave formation that are due to processes intrinsic to the cytoskeleton, cytoskeletal waves can also result from mechanic interactions with a membrane [23,24].

In this work, we consider a possible mechanism of spontaneous generation of actin bulk waves and investigate its implications on the dynamics of the membrane. We study the generation of directional cell motility through spontaneous actin waves using a mesoscopic description of treadmilling actin filaments. Motivated by the experiments in Ref. [17], we assume that filaments are nucleated by molecules that are active when bound to the substrate; see Fig. 1. Reciprocally, actin filaments induce their detachment. This system is known to generate waves provided that substrate binding of the nucleators is cooperative [20].

We consider filaments to be polar rigid rods. The distribution $c(\mathbf{r}, \hat{\mathbf{u}}, \ell)$ gives the density of plus ends at position $\mathbf{r} \in \mathbb{R}^2$ of filaments with orientation $\hat{\mathbf{u}}$ and length ℓ. The dynamic equation for c reads

$$\partial_t c = -\nabla_{\mathbf{r}} \cdot v_a \hat{\mathbf{u}} c - \partial_\ell (v_a - v_d) c - \nu_d c + \eta \nabla_{\mathbf{r}} \cdot \mathbf{f}_b c. \tag{1}$$

The first two terms on the right-hand side describe filament growth at plus ends with velocity v_a and shrinkage at

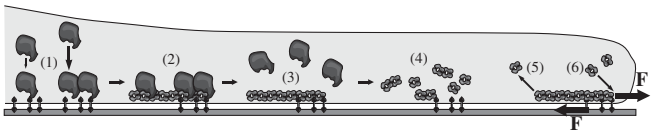

FIG. 1. Cytoskeletal processes considered in this work. Nucleating complexes bind cooperatively to the substrate (1), thus get activated, and nucleate new filaments that are linked to the substrate (2). Filaments inactivate nucleating complexes by inducing their detachment from the substrate (3). Filaments can spontaneously disassemble (4), they shrink at one end (5) and grow at the other, which generates force dipoles (6) and possible protrusion of the membrane boundary.

minus ends with velocity v_d, where $\nabla_{\mathbf{r}}$ is the two-dimensional gradient operator. Filaments degrade at rate ν_d. Generation of new filaments is captured by the boundary condition $c(\mathbf{r}, \hat{\mathbf{u}}, \ell = 0) = \nu n_b(\mathbf{r})$. Here, n_b is the distribution of active nucleating proteins and ν the nucleation rate.

Before discussing the term proportional to the force density $\mathbf{f}_\mathrm{b}$, let us note that our description neglects steric interactions and (transient) cross-links between filaments. Cross-links induce a finite elastic modulus on short time scales. For actin networks, the corresponding relaxation time is of the order of 1 to 10 s and effects on shorter time scales are not captured by our description. Steric interactions lead to confinement of filaments. We account for this effect by neglecting rotational diffusion. We also neglect translational diffusion, which would account for thermal noise and fluctuations in the polymerization and depolymerization processes. Its presence affects the dynamics quantitatively, but as long as it is below a critical value, the qualitative outcome is not changed.

The force density $\mathbf{f}_\mathrm{b}$ confines the system to an evolving domain $\Omega \equiv \Omega(t)$ with boundary $\Gamma = \partial\Omega$. We determine $\mathbf{f}_\mathrm{b}$ from a soft repulsive potential V capturing the interaction between filaments and the boundary. Explicitly, a filament with a plus end at $\mathbf{r}$ experiences a force $-\nabla_{\mathbf{r}} V(\mathbf{r}, \Gamma)$. The value of the potential at a point depends only on the (signed) distance d of the filament's plus end to the boundary Γ, $d(\mathbf{r}) = \theta(\mathbf{r}) \min_{\mathbf{r}' \in \Gamma} \|\mathbf{r} - \mathbf{r}'\|$. Here, $\theta(\mathbf{r})$ is -1 or $+1$, respectively, for $\mathbf{r}$ inside or outside of Ω. The exact form of the potential $V(d)$ is unimportant as long as it is nearly constant within most parts of the domain's interior and then rises towards the boundary. For our numerical calculations it turned out to be convenient to choose $V(d) = \alpha \tanh(\beta d)/2$ with positive constants α and β that determine the amplitude and steepness of the potential. In the limit $\alpha, \beta \to \infty$ the membrane is a perfectly reflecting boundary.

The force density $\mathbf{f}_\mathrm{b}$ is balanced by a force density $\mathbf{f}_\mathrm{env}$ resulting from interactions of the filaments with their intracellular environment. These include, notably, interactions with other cellular components and transient attachments to the substrate. They can be captured by an effective Stokesian friction force [25], $\mathbf{f}_\mathrm{env} = \eta^{-1}\mathbf{v}$, where $\mathbf{v}$ is the filament velocity and η the corresponding effective filament mobility that is much smaller than that in water. For simplicity, we assume η to be isotropic and independent of the filament length and thus arrive at the last term on the right-hand side of Eq. (1). Again for simplicity, we have neglected a possible torque exerted by the membrane on the filaments. Finally, we also neglect a dependence of the growth velocity v_a on the applied force. Taking this dependence into account does not significantly modify the solutions.

We now describe the dynamics of the nucleators. They come in two flavors: active nucleators generating new filaments are bound to the substrate, while inactive nucleators diffuse freely in Ω. The equations governing the dynamics of the corresponding densities n_b and n_f, respectively, are

$$\partial_t n_f = D_f \Delta n_f - \omega_a(1 + \omega_1 n_b^2) n_f + \omega_d T n_b, \quad (2)$$

$$\partial_t n_b = D_b \Delta n_b + \omega_a(1 + \omega_1 n_b^2) n_f - \omega_d T n_b. \quad (3)$$

The parameters ω_a and ω_1 describe attachment to the substrate, i.e., activation of the nucleators. The rate ω_d of nucleator detachment, i.e., inactivation, is proportional to the amount T of filaments at $\mathbf{r}$, $T(\mathbf{r}) = \int_0^\infty d\ell \int_0^\ell d\xi \int d\hat{\mathbf{u}} c(\mathbf{r} + \xi\hat{\mathbf{u}}, \hat{\mathbf{u}}, \ell)$. In an unbounded domain, Eqs. (1)–(3) generate a rich phase diagram presenting various traveling wave patterns as well as stationary states [20].

The structure of the dynamic Eqs. (1)–(3) allows us to integrate out the length dependence of the filament distribution. Introducing the density of plus and minus ends, c^+ and c^-, of all filaments with orientation $\hat{\mathbf{u}}$ at $\mathbf{r}$, and the total density ρ of all filaments of orientation $\hat{\mathbf{u}}$ overlapping with $\mathbf{r}$, $\rho(\mathbf{r}, \hat{\mathbf{u}}) = \int_0^\infty d\ell \int_0^\ell d\xi c(\mathbf{r} + \xi\hat{\mathbf{u}}, \hat{\mathbf{u}}, \ell)$, we obtain

$$\partial_t c^+ = -v_a \hat{\mathbf{u}} \cdot \nabla c^+ + \nu(v_a - v_d) n_b - \nu_d c^+ + \eta \nabla_{\mathbf{r}} \cdot \mathbf{f}_\mathrm{b} c^+, \quad (4)$$

$$\partial_t c^- = -v_d \hat{\mathbf{u}} \cdot \nabla c^- + \nu(v_a - v_d) n_b - \nu_d c^- + \eta \nabla_{\mathbf{r}} \cdot \mathbf{f}_\mathrm{b} c^-, \quad (5)$$

$$\partial_t \rho = -v_a \hat{\mathbf{u}} \cdot \nabla \rho + (v_a - v_d) c^- - \nu_d \rho + \eta \nabla_{\mathbf{r}} \cdot \mathbf{f}_\mathrm{b} \rho. \quad (6)$$

This simplifies the numerical solution of the dynamic equations. We provide details of the integration scheme in the Supplemental Material [26].

We now go on to present the dynamic equations governing the evolution of the boundary Γ. On each infinitesimal line element of Γ, the force is a combination of the forces exerted by the filaments as well as the force resulting from the deformation of the boundary plus dissipative forces. The deformation forces are obtained from a free energy $\mathcal{F}$ through

$$\mathbf{f} = -\frac{\delta \mathcal{F}}{\delta \Gamma}, \tag{7}$$

where $\delta/\delta\Gamma$ denotes the functional derivative with respect to variations of the boundary Γ. The expression for $\mathcal{F}$ is given by the Helfrich free energy $\mathcal{F} = \int_\Gamma d\mathbf{r}\kappa H^2/2 + \tau\Gamma + P\Omega$, where κ is the bending modulus, H the mean curvature, τ surface tension, and P the difference between internal and external pressure. By adding the interaction term $\int_\Omega d\mathbf{r}V(\mathbf{r},\Gamma)c^+_{\mathrm{tot}}(\mathbf{r})$ to $\mathcal{F}$, with $c^+_{\mathrm{tot}}(\mathbf{r}) = \int d\hat{\mathbf{u}}\, c^+(\mathbf{r},\hat{\mathbf{u}})$ being the total local density of the plus ends at $\mathbf{r}$, expression (7) also captures the forces exerted by the filaments on the membrane. Indeed, these must be of the same magnitude but of opposite orientation as the force density exerted by the membrane on the filaments to satisfy Newton's third law. The dynamic equation for the boundary is then $\dot{\Gamma} = \zeta\mathbf{f}$, where $\zeta > 0$ is an effective mobility. Equations (1)–(7) completely specify the dynamics of our system. The dynamic equations respect momentum balance: the total force exerted by the filaments on the substrate and on the membrane vanishes [26].

Our numerical analysis of the dynamic equations (1)–(7) shows that the system can spontaneously break symmetry and evolve into a state of persistent motion; see Fig. 2. For the same parameter values, the system of nucleators and filaments generates traveling wave solutions also in an unbounded domain. The propagation velocity of these free waves is larger than the migration velocity of the domain. In general, the migration velocity is bounded from above by the assembly velocity v_a and depends on the kinetics of the nucleators. It increases with the binding rate of the nucleators ω_a, but does not depend significantly on the detachment rate ω_d. Finally, the average filament length is $(v_a - v_d)/\nu_d = 1/(24\nu)$, which is much smaller than the domain size. Movies of this state and the ones discussed below are given in the Supplemental Material [26].

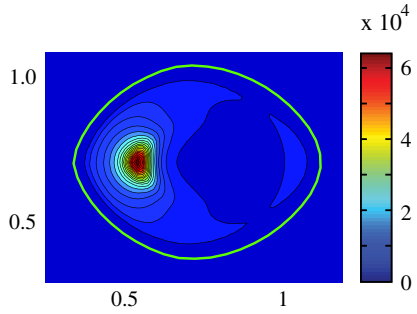

FIG. 2 (color online). Directionally moving steady state solution to the dynamic equations (1)–(7). The domain moves to the left at $v = 0.33D_f\nu \approx 2v_a/5$. Displayed is the distribution of nucleators, where the density is color coded in units of ν^{-2}. The domain boundary Γ is indicated by the full line. Parameter values are $v_d = 0$, $D = 0$, $D_b/D_f = 0.045$, $v_a/(D_f\nu) = 5/6$, $\nu_d D_f \nu^{-2} = 20$, $\omega_a/(D_f\nu^2) = 0.17$, $\omega_d/(D_f\nu^2) = 5/12$, $\omega_1\nu^4 = 3.5\times10^{-6}$, $\eta P/(D_f\nu^2) = 2\times10^{-3}$, $\tau\nu/P = 0.0075$, $\kappa\nu^2/P = 1.5\times10^{-6}$, and $n_{\mathrm{tot}} = 5000$.

We determined the phase diagram as a function of the number of nucleators and the polymerization velocity; see Fig. 3. Moving states exist above a critical number of nucleators in the domain. Furthermore, the treadmilling velocity v_a needs to be between two critical values.

For smaller values, spiral waves emerge and the system does not move on average; see Fig. 4(a). These spirals rotate with a velocity that is comparable to the propagation velocity of waves in an unbounded domain. The spirals can have multiple arms; see Fig. 4(b). Transitions between spiral states with different numbers of arms can be understood from properties of waves in unbounded domains: the corresponding wavelength λ decreases with an increasing amount of nucleators. Roughly, in the bounded domain, the transition from a one- to a two-armed spiral occurs when $2\lambda \approx 2\pi r$, where r is the average radius of the domain.

Spiral waves will generate deformations of the domain that propagate laterally along its boundary; see Fig. 5. These deformation waves are reminiscent of observations on spreading fibroblasts [27,28] and in cells of the fruit fly *Drosophila melanogaster* with an enhanced rate of actin assembly [29]. The magnitude of the domain boundary's deformation induced by a spiral wave depends on the membrane stiffness. If the stiffness exceeds a critical value, then the dynamic state of the system will change dramatically. Instead of one spiral, we then find a pair of counter-rotating spirals that send out plane waves which annihilate at the boundary [20].

Let us now return to our discussion of the phase diagram Fig. 3. Below another critical value of the assembly velocity v_a, the system settles into a stationary state, where the form of the boundary is essentially determined by its passive mechanical properties. Indeed, in this case filament growth and nucleation is too slow compared to filament degradation such that the filament density is low.

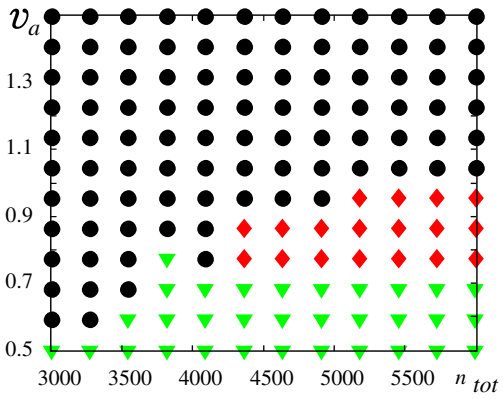

FIG. 3 (color online). Phase diagram for Eqs. (1)–(7) as a function of the total number of nucleators n_{tot} and the assembly velocity $\bar{v}_a = v_a/(D_f\nu)$. Triangles: spirals; diamonds: directional motion; dots: breathers. Other parameters as in Fig. 2.

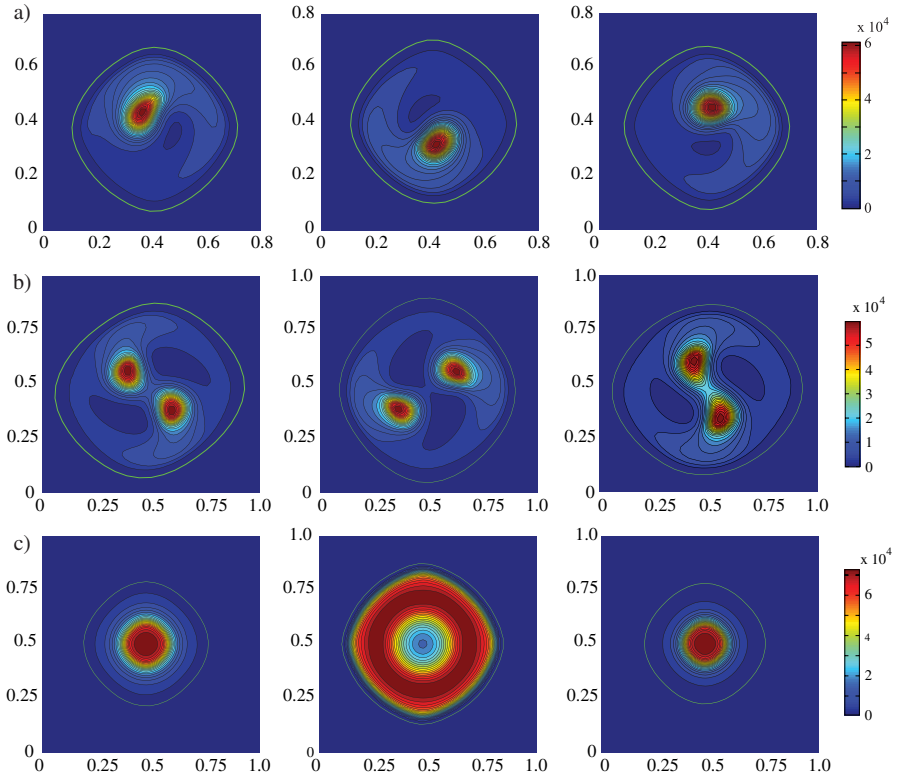

FIG. 4 (color online). Snapshots of the nucleator distribution for solutions to Eqs. (1)–(7). (a) One-armed spiral, (b) two-armed spiral, (c) breather. Clockwise rotating spirals coexist with the counterclockwise rotating spiral solutions shown in (a) and (b). Parameter values are (a) $v_a/(D_f\nu) = 2/3$, $n_{\mathrm{tot}} = 3500$, (b) $v_a/(D_f\nu) = 2/3$, $n_{\mathrm{tot}} = 6000$, and (c) $v_a/(D_f\nu) = 1$, $n_{\mathrm{tot}} = 4000$. Other parameters as in Fig. 2.

Consequently, the nucleator density is roughly homogenous, implying a uniform small ''active filament pressure'' on the boundary.

Above a critical assembly velocity, the system settles into a ''breather'' state, where the system periodically expands and deflates; see Figs. 3 and 4(c). For these values of v_a, there are no instabilities of the nucleator and hence the filament density in the orthoradial direction. Therefore, the system expands as a result of the high active filament pressure until it is so large that the nucleator density is sufficiently diluted such that the supply of new filaments is not sufficient to maintain the pressure necessary for expansion. The boundary's surface tension τ in combination with the external pressure P results in a reduction of the system size until the cycle starts anew.

Finally, let us mention that for polymerization velocities below a certain critical value, the system will collapse as the filaments cannot compensate for the external pressure.

In summary, we have presented a method to describe the dynamics of treadmilling filaments confined to a finite domain by a deformable boundary. The dynamics of the filaments is influenced by the presence of nucleators. We

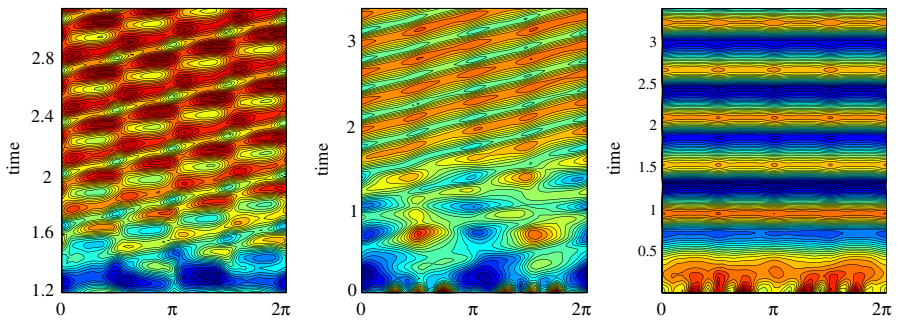

FIG. 5 (color online). Space-time plot of membrane deformations for the states shown in Fig. 4. Color coded is the deviation from a circle with its center at the position of the domain's center of mass and with radius r corresponding to the average distance of the membrane from the center $r = \int d\varphi r(\varphi)/2\pi$.

find that the system can spontaneously generate waves and that these waves can lead to directional motion of the domain. We, furthermore, find spiral waves that lead to deformation waves of the boundary and have indicated similarities with observations made on live cells. As suggested in Refs. [23,24], deformation waves could also result from instabilities of the leading edge dynamics rather than of the bulk dynamics. In general, both mechanisms can be expected to contribute to the observed dynamics. To assess their relative importance experimentally, the coupling of the cytoskeleton to the membrane should be modified.

It will be interesting to study in the future how much of cellular behavior can be understood in terms of spontaneous cytoskeletal waves. In particular, coupling our system to signal transduction pathways might shed new light on cellular responses to extracellular mechanical or chemical cues.

[1] D. Bray, *Cell Movements: From Molecules to Motility* (Garland, New York, 2001), 2nd ed.
[2] T. D. Pollard and G. G. Borisy, Cell **112**, 453 (2003).
[3] E. Sackmann, F. Kleber, and D. Heinrich, Annu. Rev. Condens. Matter Phys. **1**, 257 (2010).
[4] W. Alt and M. Dembo, Math. Biosci. **156**, 207 (1999).
[5] M. Herant, W. A. Marganski, and M. Dembo, Biophys. J. **84**, 3389 (2003).
[6] D. Bottino, A. Mogilner, T. Roberts, M. Stewart, and G. Oster, J. Cell Sci. **115**, 367 (2002).
[7] J.-F. Joanny, F. Jülicher, and J. Prost, Phys. Rev. Lett. **90**, 168102 (2003).
[8] B. Rubinstein, K. Jacobson, and A. Mogilner, Multiscale Model. Simul. **3**, 413 (2005).
[9] K. Kruse, J.-F. Joanny, F. Jülicher, and J. Prost, Phys. Biol. **3**, 130 (2006).
[10] D. Shao, W.-J. Rappel, and H. Levine, Phys. Rev. Lett. **105**, 108104 (2010).
[11] M. Sohrmann and M. Peter, Trends Cell Biol. **13**, 526 (2003).
[12] R. Wedlich-Soldner, S. Altschuler, L. Wu, and R. Li, Science **299**, 1231 (2003).
[13] A. F. Marée, A. Jilkine, A. Dawes, V. A. Grieneisen, and L. Edelstein-Keshet, Bull. Math. Biol. **68**, 1169 (2006).
[14] A. T. Dawes and L. Edelstein-Keshet, Biophys. J. **92**, 744 (2007).
[15] S. J. Altschuler, S. B. Angenent, Y. Wang, and L. F. Wu, Nature (London) **454**, 886 (2008).
[16] A. C. Callan-Jones, J.-F. Joanny, and J. Prost, Phys. Rev. Lett. **100**, 258106 (2008).
[17] O. D. Weiner, W. A. Marganski, L. F. Wu, S. J. Altschuler, and M. W. Kirschner, PLoS Biol. **5**, e221 (2007).
[18] A. E. Carlsson, Annu. Rev. Biophys. **39**, 91 (2010).
[19] K. Doubrovinski and K. Kruse, Phys. Rev. Lett. **99**, 228104 (2007).
[20] K. Doubrovinski and K. Kruse, Europhys. Lett. **83**, 18 003 (2008).
[21] S. Whitelam, T. Bretschneider, and N. J. Burroughs, Phys. Rev. Lett. **102**, 198103 (2009).
[22] A. E. Carlsson, Phys. Rev. Lett. **104**, 228102 (2010).
[23] R. Shlomovitz and N. S. Gov, Phys. Rev. Lett. **98**, 168103 (2007).
[24] M. Enculescu, M. Sabouri-Ghomi, G. Danuser, and M. Falcke, Biophys. J. **98**, 1571 (2010).
[25] K. Tawada and K. Sekimoto, J. Theor. Biol. **150**, 193 (1991).
[26] See Supplemental Material at http://link.aps.org/supplemental/10.1103/PhysRevLett.107.258103 for details of the numerical integration of the dynamic equations and movies of some solutions.
[27] G. Giannone *et al.*, Cell **116**, 431 (2004).
[28] H.-G. Döbereiner *et al.*, Phys. Rev. Lett. **93**, 108105 (2004).
[29] Y. Asano *et al.*, HFSP J. **3**, 194 (2009).